Climatic Change (2006) 78:317–340
DOI 10.1007/s10584-006-9129-z

Intra- to multi-decadal terrestrial precipitation regimes at the end of the 20th century

Steven A. Mauget

Received: 20 September 2004 / Accepted: 23 November 2005 / Published online: 13 September 2006

Abstract Intra- to multi-decadal (IMD) variation in terrestrial precipitation during 1901–98 was evaluated here by sampling annual precipitation rankings over 6–30 year moving time windows and converting those rankings to Mann-Whitney *U* statistics. Those *U* statistics were then used to identify the most significant concentrations of wet and dry years relative to a null hypothesis that assumes stationary climate variability. This time series analysis approach served as the basis of a climate survey method used to identify IMD precipitation regimes over continental areas, and was also used to evaluate IMD variation in time series of annual precipitation spatially averaged over those areas. These methods showed a highly significant incidence of wet years over North America during 1972–98, with 8 of the 10 wettest years of 1901–98 occurring during that 27-year period. A comparably significant incidence of late century wetness was also found over a northern Europe grid region, with 7 of the 10 wettest years occurring during 1978–98. Although significant wet and dry regimes were also found over other land areas in the last decades of the 20th century, the late century North American and northern European wet periods stood out as the most statistically significant found here during 1901–98. It is suggested that these recent wet periods are actually terrestrial evidence of a single multi-decadal precipitation mode extending across the North Atlantic, and the most observable evidence of an even broader pattern of recent North Atlantic climate change.

1 Introduction

When considered in terms of the surface energy budget, the Earth is a planet dominated by the influence of water. The short and long-wave reflectivities of ocean surfaces are lower than that of most natural terrestrial surface types, thus oceans are generally a more absorptive radiative sink per unit area. As oceans cover ∼71% of the Earth's surface and possessa

S. A. Mauget
U.S. Department of Agriculture-Agricultural Research Service, USDA Plant Stress and Water Conservation Laboratory, Lubbock, Texas, 3810 4th Street, Lubbock, TX 79415
e-mail: smauget@lbk.ars.usda.gov

heat capacity that dwarfs that of land surfaces and the atmosphere (Sellers 1965; Hartmann 1994), they are the leading collection and storage areas of radiative energy in the Earth's climate system. Levitus et al.'s (2001) estimates of the warming of various components of that system over the latter half of the 20th century show that the dominant increase in heat content is associated with the world's oceans. The portion of that heat content returned to the atmosphere is transferred mainly as latent heat energy, as ocean surfaces typically have low Bowen Ratios (∼.10). Such warming of the Earth's ocean-covered regions could lead to a potentially non-linear increase in atmospheric water content through the Clausius-Clapeyron equation, with an associated tendency to stronger precipitation events (Trenberth 1999; Meehl et al. 2000; Trenberth et al. 2003). As a result, telling evidence of the increased radiative forcing associated with higher greenhouse gas (GHG) concentrations or a more active sun might be found in the movement of water from and to the Earth's surface; i.e., through the hydrological cycle.

The most recent IPCC assessment of the effects of anthropogenic greenhouse gases and aerosols (Ramaswamy et al. 2001) suggests that the current net radiative forcing of those effects is approximately +1 Watt/m^2 relative to pre-industrial conditions, assuming a cooling effect of −1 Watt/m^2 from tropospheric industrial aerosols. The climate simulations of Rind et al. (2004) indicate that while the effects of increasing solar irradiance are not negligible, GHG-radiative effects dominate global warming since the Maunder Minimum period. Similarly, the results of Lean et al. (1995), Lean and Rind (1998) and Tett et al. (1999) show that while increased solar forcing may have contributed to warming in the first half of the 20th century, GHG-related warming effects dominated in the latter half. Studies of the potential effects of climate change during the 20th century have tended to focus on related variation in surface temperature (e.g., Parker et al. 1994; Easterling et al. 1994; Jones et al. 1999; Hansen et al. 2001) and the public perception of that change has centered on temperature effects ('Global Warming'). But other studies have looked for evidence of precipitation effects over varying spatial scales. Hulme et al. (1998) estimate that annual precipitation averaged over terrestrial regions has increased by approximately 2% over the 20th century, but also note a distinct drying trend in the latter half of that period. Bradley et al.'s (1987) and Diaz et al.'s (1989) trend analysis of centennial-scale zonal and hemispheric rainfall indices indicated increasing precipitation over the Southern Hemisphere, but opposing trends between subtropical and higher latitude areas of the Northern Hemisphere during the latter half of the 20th century. The similar analysis of Dai et al. (1997) also shows wetter conditions over the Northern Hemisphere poleward of 40°N and a distinct drying trend over the zonal band 0° –20°N after 1950. These broad terrestrial precipitation signals are also apparent non-zonally. Folland et al. (2001) show positive trends in annual rainfall over North America and northern Europe during 1900–1999, but negative trends over southern Europe and equatorial Africa. Over the Southern Hemisphere positive trends are evident over Australia and Argentina, but drying trends are indicated over Chile.

Over North America previous work here has shown evidence of a significantly wetter climate in the closing decades of the twentieth century. Mauget's (2003) ranking analysis of annual precipitation averaged over the continental United States during 1896–2001 revealed that 8 of the 10 wettest years occurred during the last 29 years of that 106-year period. The general occurrence of high ranked wet years during those 29 years was assigned a less than 1% probability of occurring in a stationary climate. A shift to wetter conditions is also evident in the analysis of streamflow. Lins and Slack's (1999) trend analysis showed that annually recorded low and median daily streamflow levels have increased over time over broad sections of the United States. McCabe and Wolock (2002) identified a step function increase in annual minimum and median daily streamflow levels at U.S. gage stations after

the early 1970's, which was also evident in the ranking analysis of annual mean streamflow at gage stations throughout the Mississippi River Basin in Mauget (2004) and over broader areas of the U.S. in Mauget (2003).

The significant increase in U.S. precipitation found in Mauget (2003) during the early 1970's leads to the following question: Was this increase confined to North America or was it a relatively local expression of a more widespread change in precipitation patterns? The purpose here is to address that question though a climatological survey of intra- to multi-decadal (IMD) rainfall variation over a global sampling of grid locations during 1901–98. While trend analysis of 20th century rainfall over similar grid areas have been reported elsewhere (Nicholls et al. 1996; Folland et al. 2001), the data analysis approach used here is specifically designed to identify changing precipitation patterns through the onset, duration, and significance of IMD rainfall regimes. Part 2 of this paper will discuss the data used in this analysis. Part 3 will provide a description of the time series analysis method used here, and will demonstrate that method using data from a North American grid region. Part 4 will extend the analysis to remaining areas in the northern Hemisphere, while Part 5 will evaluate southern Hemisphere areas. Part 6 will provide a summary and concluding remarks.

2 Data

The data used here was drawn from the Hulme monthly precipitation dataset (Hulme 1992, 1994; Hulme et al. 1998). This dataset reports the average monthly totals of station data over 3.75° longitude X 2.5° latitude grid regions, and was derived from a spatial averaging process using Thiessen polygon weights. Gaps in station data were filled through an anomaly interpolation method, the details of which can be found in Hulme (1999). The resulting monthly averages are reported at 1520 grid locations, but serially complete monthly data over the entire 99 year period of record (Jan. 1900–Dec. 1998) is only reported at 576 Northern Hemisphere grid locations and 150 Southern Hemisphere grid locations (Figure 1). Those grid cells account for ∼45% of total global land surface area excluding Antarctica. As a consequence, results derived here from this data can only be considered as a sampling of global terrestrial precipitation variation during the 20th century.

Although the monthly station precipitation totals contributing to these average grid values have been screened for outliers, the data has not been uniformly adjusted for time-dependent but non-climatic variation due to changes in instrumentation and/or observation practices (Groisman et al. 1991; Groisman and Legates, 1995; Peterson et al. 1998). Corrections have also not been made for the inherent tendency of rain gauges to undercatch solid precipitation, which could produce a late century warm-climate bias in precipitation measurements. That is, late-century winter warming evident over higher latitudes (Parker et al. 1994; Folland et al. 2001) could produce a widespread shift from snowfall to rainfall during the winter months. If gauge undercatch is uncorrected, such a shift would improve the meteorological network's ability to detect winter precipitation, even though total precipitation and the observing network itself were unchanged. While data from Scandinavian and Russian stations has been corrected for time dependent undercatch bias originating from changes in gauge design, such changes are not corrected for in other regions. As a result, Hulme (1999) advises caution in interpreting variation in high latitude precipitation trends outside of Russia and Scandinavia.

The climate variable considered here is annual precipitation summed over October–September water years. That integration period was chosen in order to avoid adding monthly

rainfall totals from successive wet seasons, as might occur when calendar years are used to integrate annual rainfall over Northern Hemisphere areas with winter (e.g. December–February) rainfall maximas. To avoid such a problem globally, an integration period beginning in boreal Fall/austral Spring was chosen to resolve both summer and winter precipitation maximas in either hemisphere.

3 Statistical methods and North American IMD rainfall variation

3.1 Time series analysis of running Mann-Whitney Z statistics

Low frequency variation is an important issue in climatology, but many analysis methods are poorly suited to identifying it in multi-decadal or centennial time scale data records. Although trend analysis is widely used, low frequency cyclic variation in the data can cause the significance or even the sign of trends to depend on the period over which trends are fitted (e.g., see Figure 1 and Table 1 in Hulme et al. (1998)). Fourier analysis identifies harmonic behavior, but assumes that it occurs somewhat continuously over the entire period of record. Wavelet analysis (e.g. Lau and Weng 1995) detects intermittent harmonic variation by projecting wavelet transforms onto the data over moving time windows, but is still somewhat limited by the assumption that climate varies in an idealized cyclic manner. Even so, given the intermittent nature of climate variability, moving window methods such as wavelet analysis are relatively robust. The time series analysis method used here extends the generality of wavelet analysis by making more general assumptions about how low frequency climate variability occurs; specifically, that such variation consists of non-cyclic IMD climate regimes of arbitrary onset and duration during the 20th century. The following describes this method through an analysis of spatially averaged North American annual rainfall.

Assuming an October–September summation period, 98 years of yearly precipitation (ypcp) totals can be derived for each of the 154 North American grid points in Figure 1 during January 1900–December 1998. Using those yearly totals and the areas of the corresponding equal angle grid region, a spatial average of yearly precipitation (APCP) can be estimated

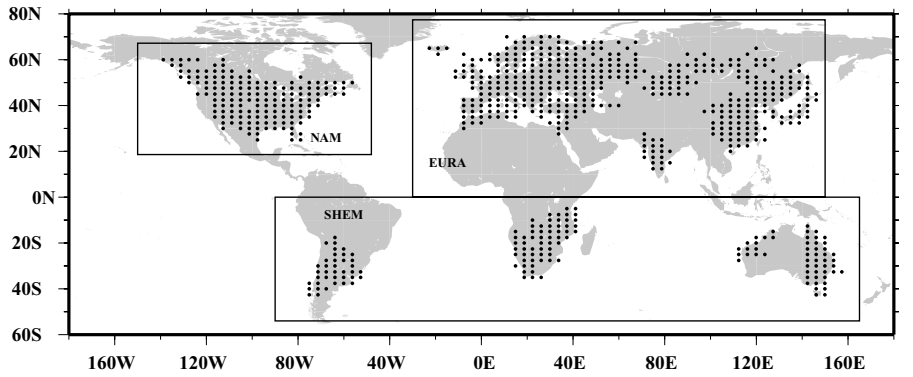

Fig. 1 Grid locations of the Hulme precipitation dataset with continuous monthly data between January 1900 and December 1999. Outlined areas mark the North American (NAM), Eurasian (EURA) and Southern Hemisphere (SHEM) grid areas considered here

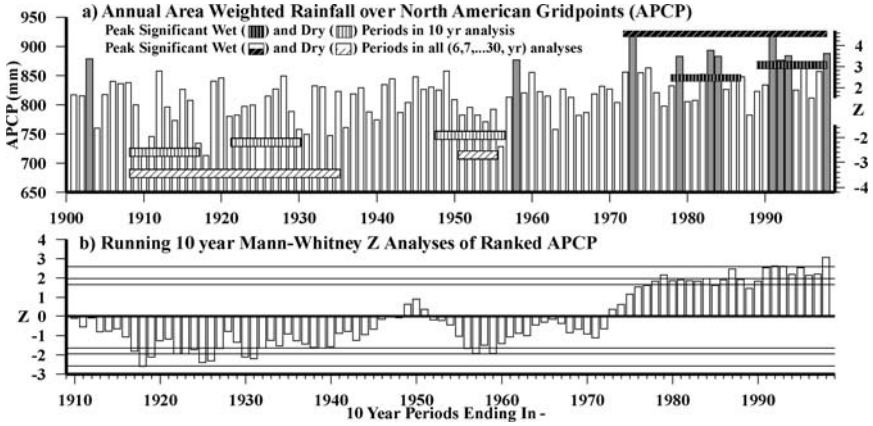

Fig. 2 (a) Time series of annual (October–September) rainfall spatially averaged over Figure 1's 154 North American grid locations for the 1901–98 water years (APCP). Gray years mark the ten most highly ranked APCP values of 1901–98. Vertically hatched horizontal bars show 10-year periods with the most significant incidence of high ($Z > 0$) and low APCP rankings ($Z < 0$) identified by the running 10 year analysis in Figure b. Oblique hatched horizontal bars show periods with the most significant incidence of high and low rankings from running analyses using sampling periods of 6,7, . . . 30 years. Vertical position of horizontal bars indicate Z values for rankings during those periods (right *Y* axis). (b) Mann-Whitney *Z* statistics for running 10 year samples of APCP rankings. Horizontal lines mark positive and negative significance at 90%, 95%, and 99% confidence levels

over those grid points.

$$\text{APCP (year } n) = \frac{\sum_{i=1}^{154} \text{area}(i) \times \text{ypcp}(i, \text{year } n)}{\sum_{i=1}^{154} \text{area}(i)} \tag{1}$$

The time series analysis approach used in Mauget (2003) and here evaluates the rankings of annual precipitation values sampled from moving time windows of varying (6–30 year) duration. The test statistic used is the Mann-Whitney *U* Statistic (Wilcoxon 1945; Mann and Whitney 1947; Mendenhall et al. 1990), which can be used to determine the significance of an arbitrary distribution of rankings in a sample. As used here, the formation of Mann-Whitney *U* statistics assumes the data has been ranked and divided into two classes. For example, the 98 years of North American APCP values in Figure 2a might be ranked and divided into a class consisting of the sample being tested (class I, of, for example, size $n_I = 10$) and the remaining non-sample rankings (class II, of size $n_{II} = 98 - n_I$). Although analytic expressions (Wilks 1995; Mendenhall 1990) are normally used to form sample *U* statistics, those statistics are equal to the total number of non-sample data values that precede each sample value when all data values are arranged by rank. That is, for the *U* statistic of the sample considered above (U_I):

$$U_I = \sum_{i=1}^{n_I} \sum_{j=1}^{n_{II}} \varphi(\text{Rank } I_i, \text{Rank } II_j), \tag{2}$$

where Rank I_i is the rank of the *i*th member of class *I*, etc., and $\phi(\text{Rank } I_i, \text{Rank } II_j) = 1$ if Rank $I_i <$ Rank II_j, 0 otherwise. Thus the maximum U_I statistic in this example would

occur when the sample accounts for the 10 highest rankings ($U_I = 88 \times 10$), while the smallest statistic would result when it accounts for the 10 lowest ($U_I = 0 \times 10$). More general sampling outcomes result in U statistics that are proportional to the incidence of high or low rankings in the sample, but bounded by those extreme values. If the 98!/88!10! possible sampling outcomes of class I rankings are equally probable, the resulting distribution of U_I statistics is Gaussian with a mean equal to the average of the maximum and minimum values (e.g., $\mu = .5^*(10 \times 88)$), and a standard deviation given by the expression $\sigma = (n_I n_{II} *(n_I + n_{II} + 1)/12)^{1/2}$ (Mann and Whitney, 1947). These parameters can be used to Z-transform U statistics, with significantly high (low) Z values indicating a significant incidence of high (low) sample rankings relative to a null hypothesis that assumes random sampling. But while climate variation can persist from year-to-year (Thiebaux and Zwiers 1984), Mann and Whitney's (1947) analytic solution for σ assumes that sampling outcomes consistent with both persistent and serially independent climate variation are equally probable. Because sampling outcomes consistent with persistent, or 'red', variation are more likely in 98-year time series of annual climate values, a more climate-specific null hypothesis will be posed here. Namely, that those time series represent a stochastic climate sharing the same mean and variance of the actual climate record, and similar persistence characteristics, but are essentially stationary and trendless during 1901–98 (H_0). From the standpoint of annual data rankings this is equivalent to assuming that high and low rankings are randomly distributed throughout time, but with persistence similar to that of the observed data. The parameters of U null distributions consistent with that hypothesis were derived here via the following Monte Carlo protocol.

I. Given a null hypothesis that assumes no long-term variation in the data, calculate AR(1), AR(2), and AR(3) regression coefficients from the autocorrelation values of the detrended data, and select the AR model yielding the minimum Akaike Information Criteria score (Akaike 1974).
II. From the results of step (i), form autoregressive red noise processes.
III. Adjust the mean and variance of the red noise process resulting from step (ii) and truncate the number of significant digits to agree with that of the data. Then, select red noise series of appropriate length – in the case of Figure 1's APCP series, 98 – and rank those values.
IV. From the ranked noise processes resulting from step (III) calculate appropriate null statistics, which in the current APCP example would be U_I statistics derived from non-overlapping 10 element segments of each red noise series.
V. Repeat (II–IV) until 50,000 independent null realizations are calculated, then determine the distribution parameters of the resulting U_I null statistics.

Using the null distribution parameters derived from these Monte Carlo simulations (μ_{MC}, σ_{MC}), the Z statistics of rankings sampled from the un-detrended APCP time series can be used to test H_0.

$$Z = \frac{U - \mu_{MC}}{\sigma_{MC}} \tag{3}$$

The Mann Whitney Z statistics for running 10-year samples of ranked North American APCP values can be found in Figure 2b. Generally, these running analyses tend to produce redundant results at a fixed sampling size (n_I). For example, of the nineteen 10-year sampling periods that begin after 1970, all but 2 (1976–85, 1980–89) are positively significant at a 90% confidence level ($Z > 1.645$). To isolate the most significant IMD variation occurring over

distinct periods, the approach here is to identify only the most significant sequences of rankings exceeding a minimum 90% confidence threshold ($|Z| > 1.645$) and occurring over non-overlapping time windows. Thus in Figure 2a the distinct and optimally significant dry periods marked by the 10-year analysis are 1909–18 ($Z = -2.594$), 1922–31 ($Z = -2.203$) and 1948–57 ($Z = -1.916$). The significantly wet 10-year periods identified are 1978–87 ($Z = 2.458$) and 1989–98 ($Z = 3.055$).

Because the running analysis leading to Figure 2a evaluates Mann-Whitney U statistics over all possible 10-year windows, optimally significant wet or dry periods occurring over any 10-year time window can be identified during 1901–98. To extend this test to a wider range of time scales running calculations of U statistics were repeated using sample sizes of 6,7, ... 30 years. Varying sample size required that Equation 2's μ_{MC} and σ_{MC} parameters be calculated for each window length, given the dependence of those parameters on sample size. Thus μ_{MC}-σ_{MC} parameter pairs were calculated independently for each of the 25 sample sizes in the course of the Monte Carlo simulations. After the running U statistics from each analysis were normalized by the appropriate null parameters (Equation 3) the Z statistics from all 25 tests that exceeded the minimum confidence threshold were, as in the 10 year analysis, screened for those periods resulting in the greatest significance over non-overlapping IMD periods. Thus the most significant negative Z statistic (−3.450) from all 25 running analyses of APCP rankings is found in the 28 year analysis during 1909–36. This result effectively trumps both the 1909–18 and 1922–31 Z statistics from the 10-year analysis and all other significant Z statistics from sampling periods that overlapped 1909–36. Similarly, the Z statistic from the 6-year analysis during 1951–56 (−2.700) exceeds the 1948–57 10 year Z statistic, and all other Z statistics that showed dry conditions during the early 1950's over other time windows. The most significant positive Z statistic (4.584) among all analyses, and the greatest magnitude statistic overall, is evident during the 27 year period 1972–98. That statistic's magnitude allows for the rejection of the previously described null hypothesis (H_0) at a 99% confidence level and shows an unprecedented concentration of high ranked APCP values after 1971. Like a comparable result in Mauget (2003) derived from United States climate division precipitation data, that statistic is strongly influenced by the fact that 8 of the 10 wettest years in Figure 2a's precipitation record are found during the final 30 years of the 20th century.

3.2 IMD climate survey method

Testing spatially averaged precipitation time series using Section 3.1's method is useful over land areas that share a coherent IMD climate response. Over North America this is known to be the case during recent decades from previous work. But over larger geographic regions such as Eurasia different areas could experience simultaneous dry and wet IMD periods. Under such circumstances, spatially averaging across arbitrary land areas (e.g. Vinnikov et al. 1990; Groisman and Easterling 1994), or across land areas within a zonal band (e.g., Diaz et al. 1989; Dai et al. 1997) might cancel out those opposing climate signals. To isolate the timing of wet or dry IMD regimes and the areas over which they occur, an additional survey method will be used here which basically reverses the process described in Section 3.1. That is, whereas before spatial averaging was followed by running Z analyses of the resulting time series, this method first conducts running analysis of ranked annual data from individual grid locations, then records the percentage of total grid area that shows significant positive and negative Z statistics during running time windows. The method used to test samples of rankings at the grid level is identical to that used to test U statistics derived from running samples of APCP rankings. Null U distribution parameters are determined via the

Monte Carlo process described before, with μ_{MC} and σ_{MC} parameters derived for annual rainfall series at each grid location.

An example of this survey approach can be found in Figures 3a and 3b. Figure 3a shows the North American area percentages that result when annual rainfall rankings over all 27-year sampling windows during 1901–98 are tested for positive significance ($Z > 1.645$). As in Figure 2a, the 1972–98 result is the maximum value, with approximately 48% of the North American grid area showing a significant incidence of highly ranked annual rainfall. In Figure 3b triangles mark those grid locations whose *Z* statistics for 1972–98 annual rainfall rankings are positively significant at a 90% level or better, with darker shades showing higher significance. Significant negative *Z* statistics – which are marked by inverted triangles of various shades – are limited to grid locations in western Canada.

As in Section 3.1, this survey method is extended to a wider range of IMD time scales by using sampling windows of varying duration. Thus analyses similar to that leading to Figure 3a were conducted with 25 sample window sizes between 6 and 30 years in length. This varying window duration required Monte Carlo trials to be repeated for each window length, given the dependence of μ_U and σ_U on sample size. Thus for each grid location, 25 μ_{MC}-σ_{MC} parameter pairs were independently generated through the course of the Monte Carlo simulations. For each of the 25 sample window sizes, running analyses of significant positive and negative annual rainfall Z statistics over the North American grid locations produced 2 area timelines similar to Figure 3a, resulting in a total of 50 timelines. Again, the peak values in these timelines indicate *n*-year periods during which relatively large areas of North America experienced a significant incidence of low (MWZ < -1.645) or high (MWZ $>$

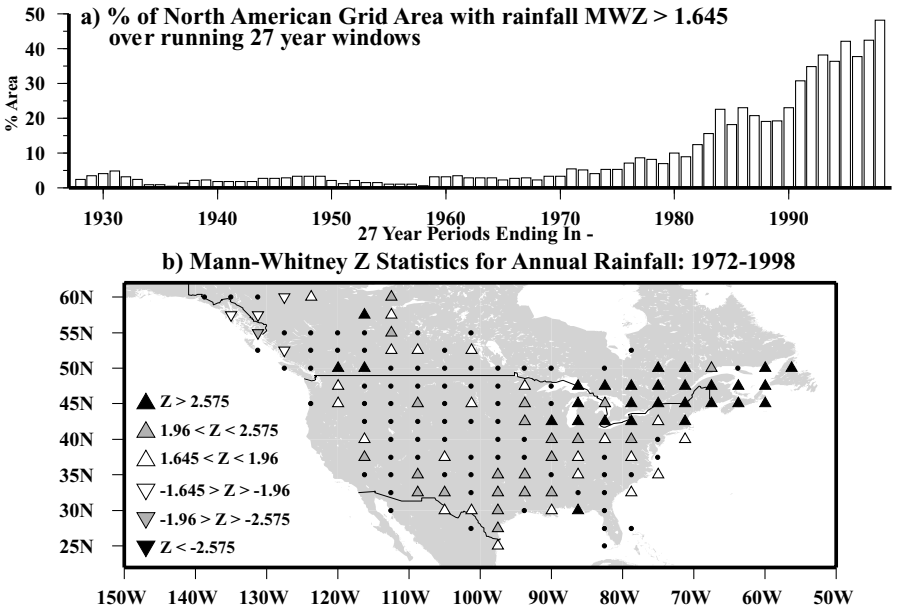

Fig. 3 (a) Percentage of North American grid area showing positively significant (>1.645) Mann Whitney *Z* statistics for October-September rainfall over running 27 year time windows during 1901–98. (b) *Z* statistics for annual rainfall rankings at each grid location during 1972–98. Progressively shaded triangles (inverted triangles) show positive (negative) Z statistics significant at 90%, 95%, and 99% confidence levels

1.645) rankings in annual rainfall relative to H_0. Given the number of timelines generated, only the peak periods are shown here in Figure 4a and 4c.

In Figure 4a black bars show the peak wet periods at each sample size. The gray bars in that figure mark secondary peak periods, defined here as time windows during which significant Z statistics were found over areas comparable to peak area values, but did not overlap the primary peak period in time. Comparable areas were considered here as at least 70% of the peak period area. Similarly, the black and gray bars in Figure 4c mark IMD dry periods. The corresponding percentage of total North American grid area exhibiting significant positive and negative Z statistics during each primary peak time window are found in Figures 4b and 4d. As a result, the peak percentage for the 27-year analysis in Figure 3a during 1972–98 is found again in the 27-year analysis of Figure 4b. Figures similar to Figure 4 will be used here as departure points in the following climate survey method:

- Peak area values found in Figures b and d of those figures are first used to identify the sampling window size that resulted in the most spatially extensive climate impacts, with the corresponding black bars in Figures a and c marking time windows during which the impacts occurred.

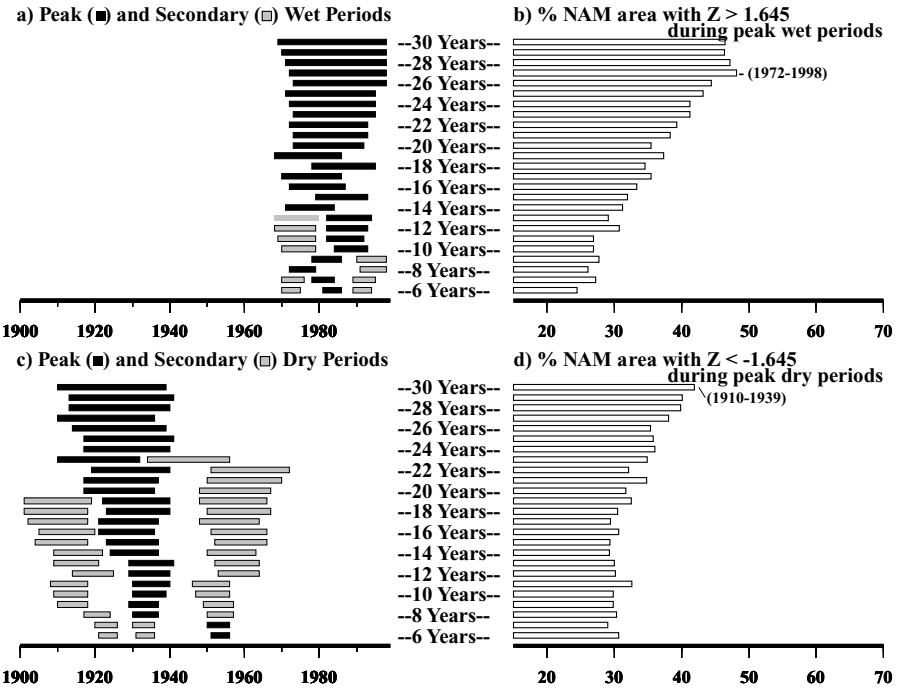

Fig. 4 (a) N-year time windows during which relatively large areas of North America (NAM) grid locations experienced a significant incidence of high ($Z > 1.645$) rankings in annual rainfall, as determined by timelines similar to Figure 3a. Black bars show peak wet periods at each sample size for $N = 6$ to 30 years. Gray bars mark secondary peak periods, defined here as periods during which significant Z statistics were found over areas comparable to peak area values, but not overlapping the primary peak period in time. (b) Percentage of total North American grid area showing significance at a 90% or better confidence level during the corresponding peak wet periods in (a). (c) As in (a) for peak and secondary periods marked by a significant incidence of low (i.e., $Z < -1.645$) rankings in annual rainfall. (d) Percentage of North American area grid showing significant Z statistics during corresponding peak dry periods in (c)

- Over those time windows, Z mappings similar to Figure 3b are then plotted to determine the areas affected during those dry or wet periods.
- Finally, APCP time series similar to that of Figure 2a are formed over those areas, and the time history of the area's IMD variation is further evaluated using the method of Section 3.1.

This climate survey process is objective and robust because it is based on a time series analysis method that possesses those properties. The method of Section 3.1 is robust because it is based on a non-parametric test that is insensitive to assumptions of distribution. The Mann-Whitney U statistic is also objective in that it can identify runs of extreme rankings, but imposes no artificial thresholds that define extreme rankings. By repeating that test over running time windows of varying duration, the survey method used here can objectively determine when, where, and at what significance IMD precipitation regimes have occurred over specified grid regions during 1901–98.

4 Other northern Hemisphere IMD rainfall variation

Figure 5 is the counterpart to Figure 4 calculated over Figure 1's 421 Eurasian (EURA) gridpoints. Like Figure 4a's North American survey, many periods of peak wetness occur during late century time windows, with the most spatially extensive wet period occurring during 1980–98. But unlike the North American results, earlier periods of wetness during the early and mid-20th century were comparable in their areal coverage over this extensive land area. In the 14-year analysis the peak wet period was 1908–21, and the map of those years Z statistics (not shown) show wet conditions over China and the eastern Mediterranean. Over the 6–12 year sampling windows peak wet periods occur during mid-century, with the most widespread effects found during 1956–64. A map of the Z statistics during that 9-year period (not shown) shows wet conditions over India and east Asia. In Figure 5c almost all primary dry peak periods occur during early century time windows. However, in Figure 5a those approximate time windows are also shown as secondary wet periods, which shows that wet and dry conditions co-existed over the EURA region during the early 20th century. Evidence of simultaneous wet and dry IMD periods are also apparent during the late 20th century in Figures 5a and 5c, as secondary dry periods in Figure 5c during late century 8–16 year time windows approximately coincide with primary wet periods in Figure 5a.

Figure 6 is the EURA counterpart to Figure 3b, with Z statistics plotted for annual rainfall rankings at each grid location during 1980–98. Apart from relatively scattered evidence of wetness over the outlined east Asian (E-ASIA) grid cells, that figure is dominated by a pattern of opposing rainfall regimes over Europe. A significant incidence of wet years is apparent at most grid points within the outlined northern European (NEUR) region which includes the British Isles, Scandinavia, and the western 1/3rd of Russia. By contrast, many southern European (SEUR) gridpoints outlined in Figure 6 show a significant incidence of low ranked annual rainfall conditions over southern and central Europe, the Balkans, and the Mediterranean.

Figure 7a is analogous to Figure 2a, with annual rainfall spatially averaged over Figure 6's NEUR gridpoints during 1901–98. As in Figure 2a the horizontal bars of Figure 7a mark periods with the most significant incidence of high and low rankings from running analyses of MWZ statistics using sampling periods of 6,7, ... 30 years, and the vertical placement of those bars mark the corresponding Z values for rankings during those periods. Figure 7a shows an apparently abrupt shift to wetter conditions over Figure 6's NEUR region during

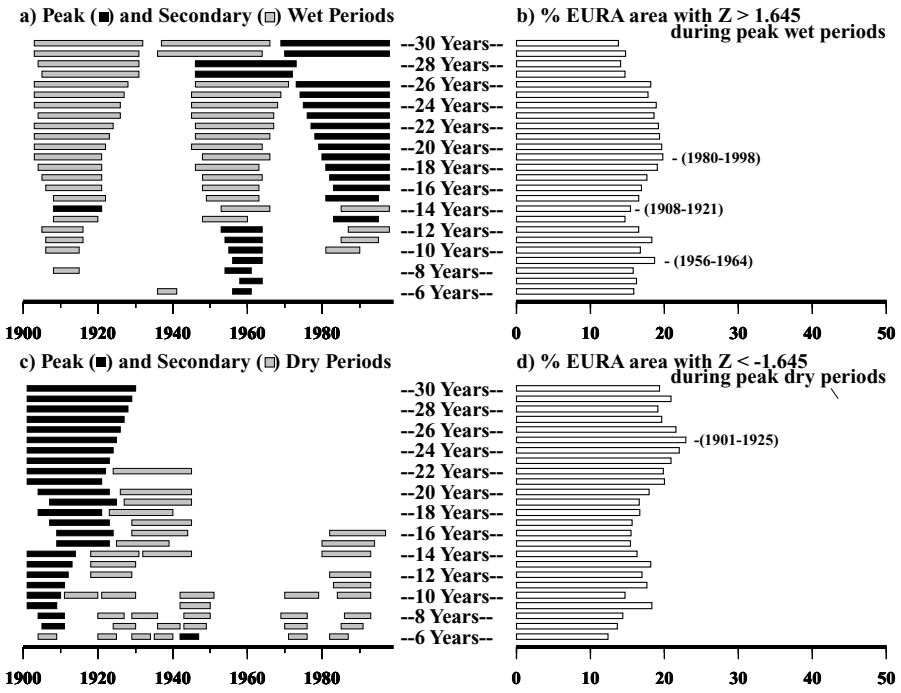

Fig. 5 As in Figure 4a–d for the 421 grid locations of the EURA area in Figure 1

1978–98, similar to that found in Figure 2a's North American time series. During that 21-year period 17 years ranked above the 98-year median northern European APCP value, and 7 of those years were among the 10 wettest years of 1901–98. The resulting *Z* statistic (4.680) marks the most significant concentration of wet or dry years in the Figure 7a time series.

Figure 7b's is Figure 7a's counterpart over Figure 6's SEUR gridpoints during 1901–98, and shows a late-century transition in IMD rainfall roughly opposite to that found over northern Europe. That is, whereas Figure 7a shows a transition from significantly dry conditions during 1969–76 to significantly wet conditions during 1978–98, wet conditions over the southern European gridpoints during 1958–81 gave way to dry conditions during 1982–93. However, there is also evidence of a recent recovery from that latter dry period, as the 1995–98 southern European APCP values have ranked above the 1901–98 median (>49).

To compare the significance of the recent northern European wet period with other Eurasian wet periods during 1901–98, figures analogous to Figure 2a for APCP averaged over Figure 6's east Asian, India (IND) and China (CH) gridpoints can be found in Figures 8a,b, and c. In Figure 8a a recent wet period is evident in the east Asian APCP record during 1981–98, but the magnitude of the associated Z statistic (2.090) shows the roughly concurrent northern European wetness to be the stronger IMD climate effect. As mentioned earlier, the Eurasian climate survey marked the late 1950's and early 1960's as a wet period over east Asia and India, which is evident in Figures 8a and b. In the east Asia APCP series 5 of the 10 wettest years of 1901–98 occurred during 1955–62, leading to a Z statistic of 3.360. In the India APCP time series the incidence of high ranked annual rainfall conditions during 1954–63 produces a comparable *Z* statistic (3.285). Figure 8c shows recent evidence of a

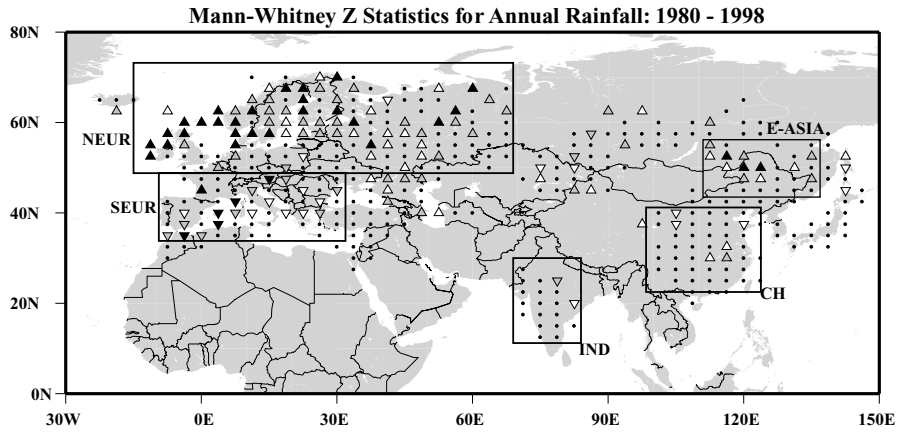

Fig. 6 Mann-Whitney Z statistics for annual rainfall rankings at each Eurasian grid location during 1980–1998. Outlined areas mark the northern European (NEUR), southern European (SEUR), east Asian (E-ASIA), India (IND) and China (CH) gridpoint regions referred to in the text. Positive and negative significance of Z statistics is marked by the token shading scheme of Figure 3b

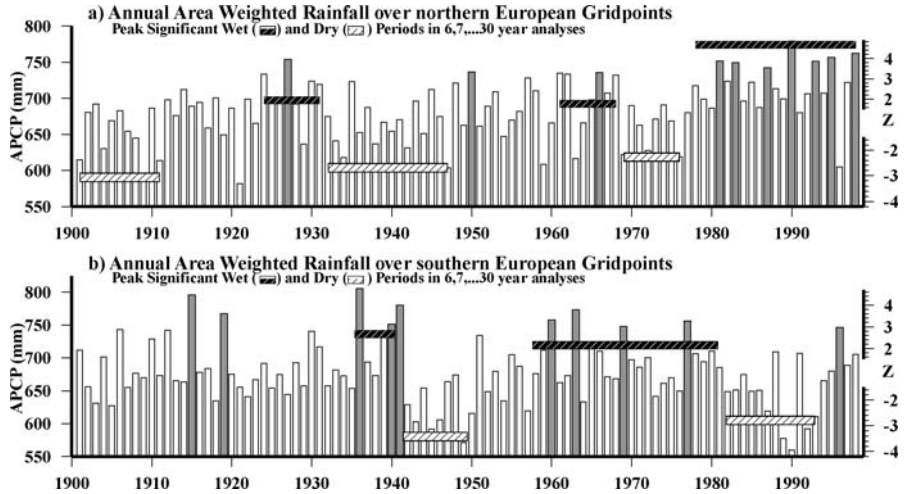

Fig. 7 (a) Time series of annual (October–September) rainfall spatially averaged over Figure 6's NEUR grid locations for the 1901–98 water years (APCP). Gray years mark the ten most highly ranked APCP values of 1901–98. Oblique hatched horizontal bars show periods with the most significant incidence of high and low rankings from running analyses using sampling periods of 6,7, . . . 30 years. (b) As in (a) for Figure 6's SEUR grid locations

shift to wetter conditions over China, with the relatively dry 1978–89 period giving way to weakly significant wet conditions during 1992–98 ($Z = 1.747$). But wet periods of greater significance are found in the China APCP series during 1903–21 ($Z = 2.989$) and 1945–54 ($Z = 2.533$). Overall, Figures 7 and 8 show that while IMD wet periods have occurred throughout the EURA grid region during the 20th century, the recent northern European wet period is clearly the most significant.

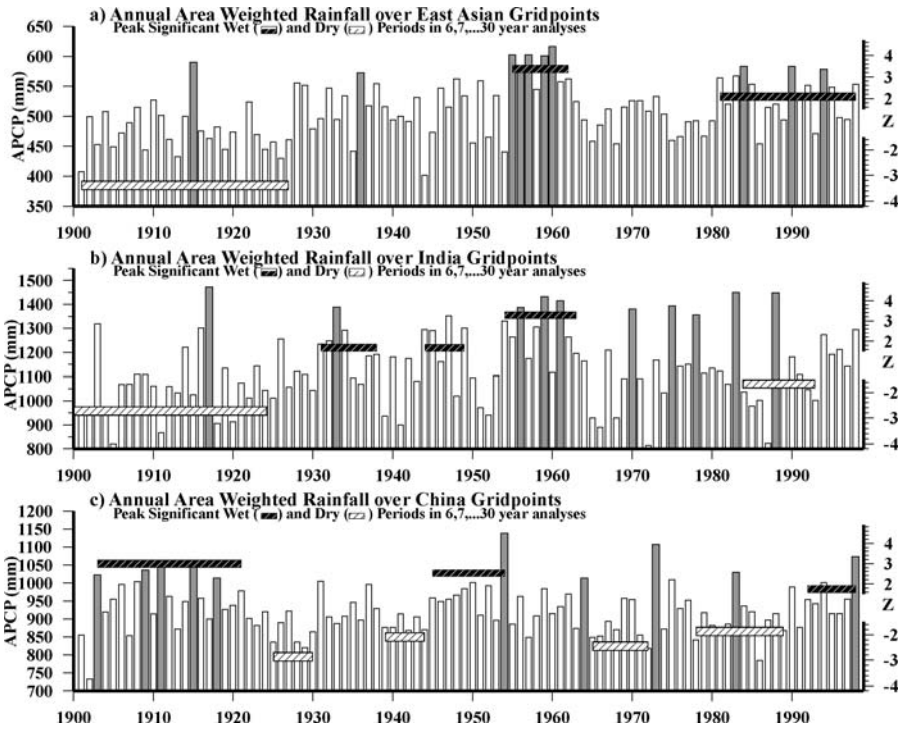

Fig. 8 (a) As in Figure 7a for Figure 6's E-ASIA grid locations. (b) As in Figure 7a for Figure 6's IND grid locations. (c) As in Figure 7a for Figure 6's CH grid locations

5 Southern Hemisphere IMD rainfall variation

Figure 9 is the result of integrated MWZ analyses similar to those that produced Figures 4 and 5 as applied over all of Figure 1's SHEM grid areas. Like the corresponding North American results in Figure 4a all peak wet periods in Figure 9a occur after mid-century, and all but 2 begin after 1971. Figure 9b shows that the most spatially extensive of these wet periods occurred during 1974–79. Figure 9c reveals 2 general periods of extensive Southern Hemisphere dryness over land. In Figure 9d the 20–30 year periods of peak dryness are found between the early 1920's and the late-1940's, with 1923–49 marked as the time of most widespread dryness. In the 9–19 year analyses the peak dry periods all begin after 1979, with the most extensive effects occurring during 1982–96. As a result of these more recent dry periods, Figures 9a and c show both wet and dry IMD periods over the Southern Hemisphere grid regions in the last decades of the 20th century. This in turn suggests late-century IMD rainfall regimes of opposite sign over South America, southern Africa, and Australia, which are illustrated in Figure 10a and 10b.

Figure 10a is a plot of the MWZ statistics for annual rainfall rankings at each Southern Hemisphere grid location during 1974–79, and shows that wet conditions were widespread over southern Africa and eastern Australia during that time and somewhat less evident over South America. Figure 10b shows that during 1982–96 dry conditions were limited to southern Africa, but that South American wet conditions became more widespread.

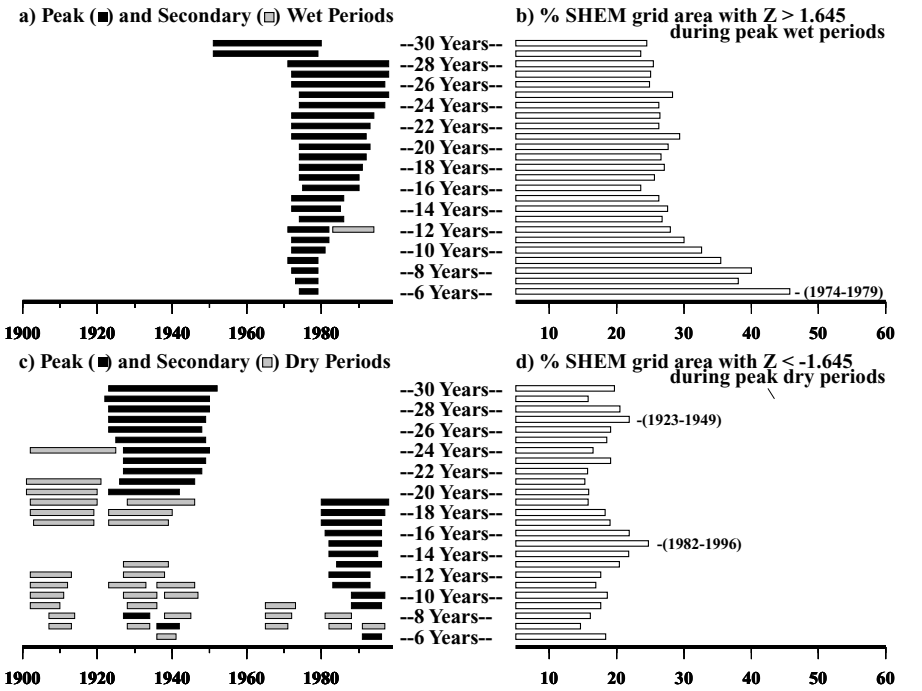

Fig. 9 As in Figure 4a–d for the 150 grid locations of the Southern Hemisphere (SHEM) area in Figure 1

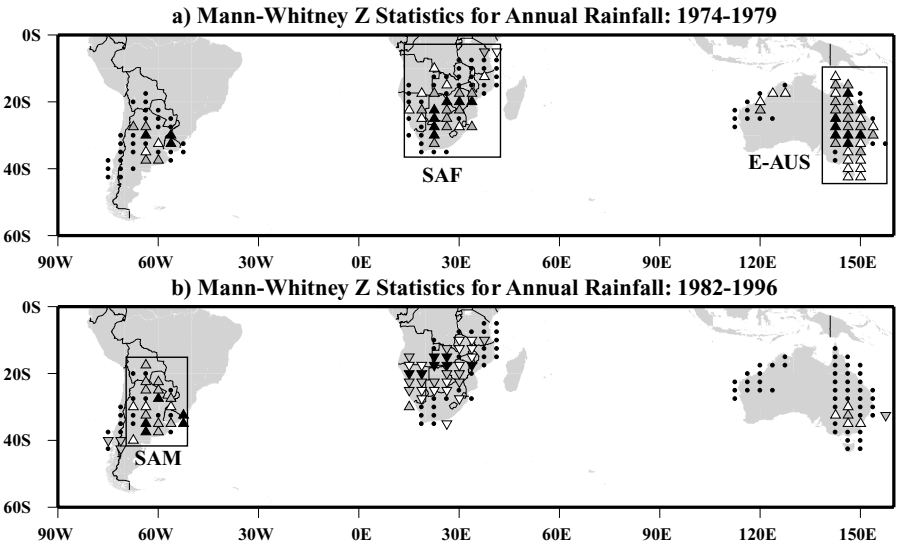

Fig. 10 (a) Mann Whitney *Z* statistics for annual rainfall rankings at each SHEM grid location during 1974–79. (b) Z statistics for annual rainfall rankings at each SHEM grid location during 1982–96. Outlined areas mark the South American (SAM), southern African (SAF), and eastern Australian (E–AUS) grid regions referred to in the text

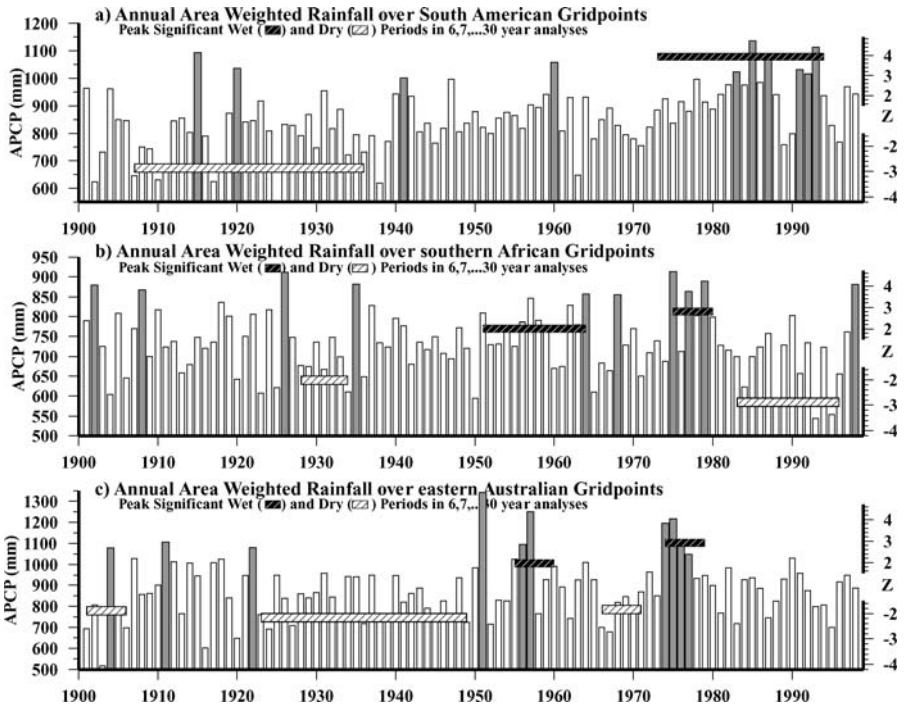

Fig. 11 (a) As in Figure 7a over Figure 10's SAM grid locations for the 1901–98 water years. (b) As in Figure 7a for Figure 10's SAF grid locations. (c) As in Figure 7a for Figure 10's E-AUS grid locations

The time series of spatially averaged annual rainfall over Figure 10's South American (SAM), southern African (SAF), and eastern Australian (E-AUS) grid points can be found in Figure 11a–c, together with the optimally significant dry and wet periods found by running *Z* analyses. In Figure 11a those analyses marked 1973–94 as the most significant wet period over the South American grid regions. An only slightly less significant South American wet period occurred during 1974–98, but the lower *Z* statistic for that period in the 25-year analysis (3.899) was trumped by the 1973–94 statistic (3.914) in the 22-year analysis. As a result, a significant tendency to end of century wetness was found over the SAM grid area, but this wet period was tempered by low ranked annual rainfall conditions in 1989, 1990, and 1996. Figure 11b's southern African time series shows a transition from significantly wet conditions during 1975–80 to dry conditions during 1983–96. It is interesting to note that the shift from wet to dry conditions over southern Africa during the early 1980's in Figure 11b was roughly in phase with a similar shift over southern Europe in Figure 7b, which was in turn coincident with the shift from dry to wet conditions over northern Europe in Figure 7a. This suggests a roughly simultaneous inter-hemispheric response in the general circulation over the longitudes spanned by Figures 6 and 10's European and southern African grid areas. Figure 11c shows that, like southern Africa, extremely wet conditions were evident over Figure 10a's eastern Australia grid points during the mid- to late 1970's. However, unlike southern Africa, no significant incidence of low ranked rainfall is evident over that region after the early 1980's.

6 Summary and discussion

Rankings of annual (October–September) precipitation totals calculated over a global sampling of terrestrial grid locations (Figure 1) during 1901–98 were subjected here to time series analysis of Mann-Whitney *U* statistics over running intra- to multi-decadal (IMD) sampling windows. As the magnitude of *U* statistics are proportional to the incidence of high or low rankings during a sampling period, such running analyses can identify the most statistically significant sequences of extreme annual rankings in a data record at a fixed sample size. Repeating these analyses over sample sizes of 6–30 years allows for the objective identification of IMD precipitation regimes of arbitrary onset and duration in the data record. This approach was applied here at two levels: 1) to time series at the grid level as part of a climate survey process that identified when and where IMD rainfall regimes occurred over continental and hemispheric land regions (Section 3.2; Figures 4, 5, 9), and, 2) to time series of annual precipitation spatially averaged over grid areas determined by that survey to share a significant IMD response (Section 3.1; Figures 2, 7, 8, 11).

This research follows earlier work (Mauget, 2003) that showed a highly significant shift to wetter conditions over the continental United States after the early 1970's, also found here in Figures 2 and 3. The main question posed here was whether that wetness was limited to North America or was a regional expression of a more widespread shift in global precipitation. The answer to that question is that while recent precipitation increases were found over some terrestrial areas, wetter conditions of even greater significance were found over northern Europe after the late 1970's. Other land areas where recent wetness was evident were the southern portion of South America (Figure 10b, 11a), east Asia (Figure 6, Figure 8a) and China (Figure 8c). A nearly concurrent shift to dry conditions was found in both southern European (Figure 7b) and southern African (Figure 11b) precipitation after 1980, but neither dry period persisted until the end of the data record (1998). Over the eastern Australia region considered here no significant incidence of low or high ranked annual rainfall conditions was apparent at the end of the century (Figure 11c).

In terms of conditions averaged over geographic areas, the most statistically significant concentrations of high ranked annual precipitation during 1901–98 were found over northern Europe during 1978–98 and over North America during 1972–98 (Table 1). The recent opposing decadal precipitation regimes shown here over northern and southern Europe in Figures 6 and 7 have been reported by Hurrell (1995) and Hurrell and van Loon (1997), who attribute them to the persistent positive phase of the North Atlantic Oscillation (NAO) that has existed since the early 1980's. The NAO is a central influence on North Atlantic climate that is most dynamically active during the winter months (Hurrell et al. 2003). It can

Table 1 Wettest periods during 1901–98 by grid region

Grid Region	Period	MWZ
Northern Europe	1978–98	4.680
North America	1972–98	4.584
South America	1973–94	3.914
East Asia	1955–62	3.360
India	1954–63	3.285
China	1903–21	2.989
Eastern Australia	1974–79	2.909
Southern Africa	1975–80	2.804
Southern Europe	1936–41	2.659

Intra to multi-decadal periods of peak wetness over the regional grid areas considered here, as determined by running Mann-Whitney Z analysis of spatially averaged annual rainfall

influence winter precipitation patterns from North America to Europe and the Middle East through the meridional displacement of the North Atlantic storm track (Hurrell 1995; Hurrell and van Loon 1997; Hurrel et al. 2003). During the mode's negative phase (NAO-) the storm track assumes a relatively direct course between the eastern coast of the United States and the Mediterranean. The mode's positive phase (NAO+) moves the storm track northwards, with a consequential drying effect on the Mediterranean and the Middle East (Cullen and deMenocal 2000; Eshel et al. 2000; Cullen et al. 2002). That displacement also produces more southwesterly moisture transport across eastern North America and the North Atlantic that penetrates northward into northern Europe and Scandinavia (Hurrell 1995; Dai et al. 1997). Through the use of gridded precipitation analyses (Dickson et al. 2000; Cullen et al. 2002, see Figure 12) and the calculation of atmospheric moisture budgets in the NCEP/NCAR reanalysis (Hurrell 1995; Hurrell et al. 2003; Visbeck et al. 2003) the positive mode has also been shown to increase winter precipitation over the northern North Atlantic. The patterns of Z statistics outlined in Figures 13a and 13b mark NAO+ moisture advection over land areas, with highly significant incidences ($Z > 2.545$) of wet years at the North American entrance and Scandinavian exit regions of the North Atlantic storm track during recent decades. Given these terrestrial rainfall patterns, and the trans-oceanic extent of the North Atlantic storm track (Rogers 1990, 1997; Hurrell et al. 2003), two indirect conclusions are proposed here: (1) that these recent wet regimes are most likely terrestrial evidence of a single multi-decadal wet mode extending from eastern North America to Scandinavia and beyond, and (2), that similar wet conditions may have occurred over the North Atlantic.

The time series of annual rainfall averaged over Figure 13a and b's entrance and exit grid regions can be found in Figures. 13c and d, and show increases of 10.5% and 7.3% respectively during recent decades relative to previous years. Assuming that conditions over those regions are roughly representative of North Atlantic conditions, this suggests that North Atlantic rainfall may have increased by ∼7–10% since 1980. Increased North Atlantic rainfall rates could have important climatic consequences, as these ocean areas include deep-water formation sites of the thermohaline circulation (Broecker and Denton 1989; Broecker 1997). Modeling simulations (Stocker and Wright 1991; Rahmstorf 1994) show that reductions in North Atlantic salinity and surface density could, by slowing or stopping that circulation, lead to abrupt cooling of North Atlantic climate. Recent decades have seen a tendency to lower salinity conditions over the North Atlantic that were dominant during the 1970's (Dickson et al. 1988; Dickson 1995; Hansen and Bezdek 1996; Curry and Mauritzen 2005), and were also evident during the 1980's (Curry and Mauritzen 2005) and 1990's (Häkkinen 2002). After evaluating multi-decadal oceanographic records, Curry and Mauritzen (2005) conclude that that an equivalent freshwater layer ∼3.0 m thick has been introduced into the North Atlantic during 1965–95, over an ocean area roughly extending between Figure 13's entrance and exit regions. Broecker (1997) estimates that if the excess of precipitation plus runoff over evaporation were to increase by 50% over the North Atlantic, the winter surface waters from which deep water formed would have to cool by 1.4°C to compensate for the resulting reduction in density. However, given the transition to cooler North Atlantic sea-surface temperatures after the early 1970's (Schlesinger and Ramankutty 1994; Hansen and Bezdek 1996; Sutton and Allen 1997), such compensation may be occurring.

The recent tendency to cooler and fresher North Atlantic ocean conditions might be traced to multiple influences including increased flow of fresh water and ice from the Arctic, decrease of saline water northward from the subtropical Atlantic and increased precipitation (National Research Council 2002; Dickson et al. 2002). Of these influences the first suggests the effects of Arctic warming (Rothrock et al. 1999; Serreze et al. 2000; Comiso and

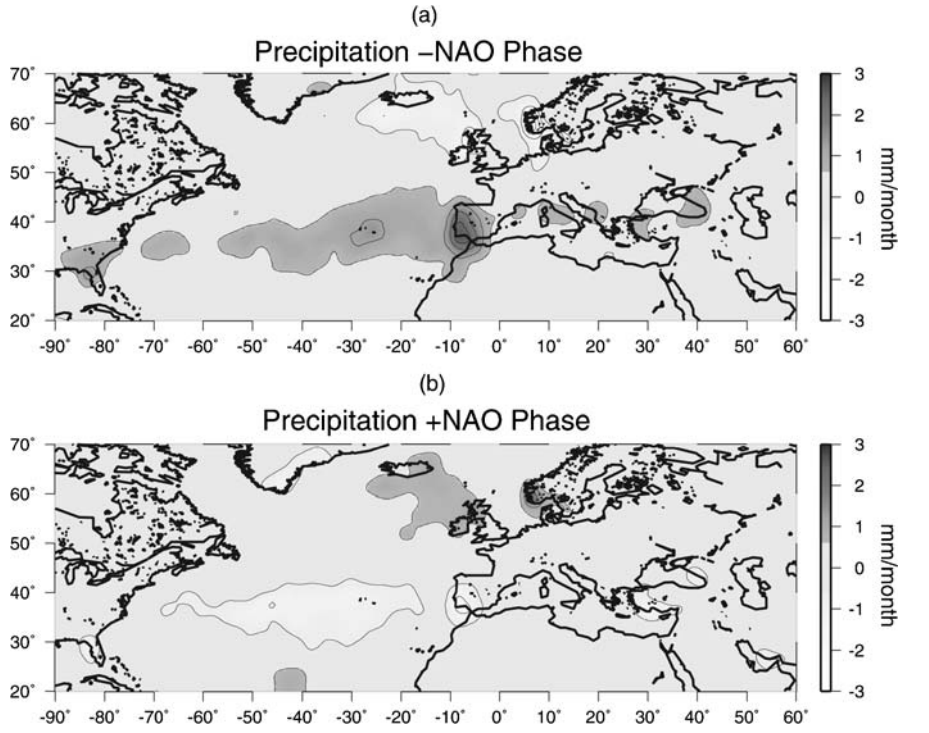

Fig. 12 Composite winter (December–March) precipitation anomalies derived from CMAP monthly data (Xie and Arkin, 1996) for (a) negative phase NAO conditions, and (b) positive phase NOA conditions (From Cullen et al. 2002)

Parkinson 2004), while the last suggests increased rainfall over the North Atlantic storm track. The latter possibility and the recent precipitation increase proposed here are indirectly supported by Curry et al.'s (2003) ocean salinity analysis, which shows salinity increases in the northern subtropical Atlantic and decreases at higher latitudes between the 1950's and 1990's. Because the salt content of ocean basins is roughly conserved, these salinity changes are consistent with the net transfer of fresh water from subtropical to mid-latitudes over the North Atlantic through increased evaporation and precipitation rates. The results found here suggest that increased precipitation may have contributed substantially to the recent North Atlantic freshening. Assuming a rainfall increase over Curry and Mauritzen's (2005) sub-polar basin region (see Figure 13a, and b) during 1980–95 equal to Figure 13d's post-1979 step increase, then the annual rainfall over that ocean area may have increased by an average of 70 mm during those 16 years relative to 1901–79. Cumulatively, that would result in an addition of ∼1.0 meter of freshwater during 1980–95, approximately one-third of Curry and Mauritzen's 3.0 meter estimate during 1965–95.

Curry et al. (2003) note that subtropical North Atlantic water masses were both warming and becoming more saline and evaporative in recent decades, and suggest that this may be a consequence of a stronger hydrological cycle and broader trends of global warming. Dickson et al. (2000) have also proposed a recent shift in the North Atlantic hydrological cycle. Their study of the Xie and Arkin (1996) precipitation analyses shows increased precipitation over the Norwegian and Greenland seas during NAO+ conditions. Given the pronounced

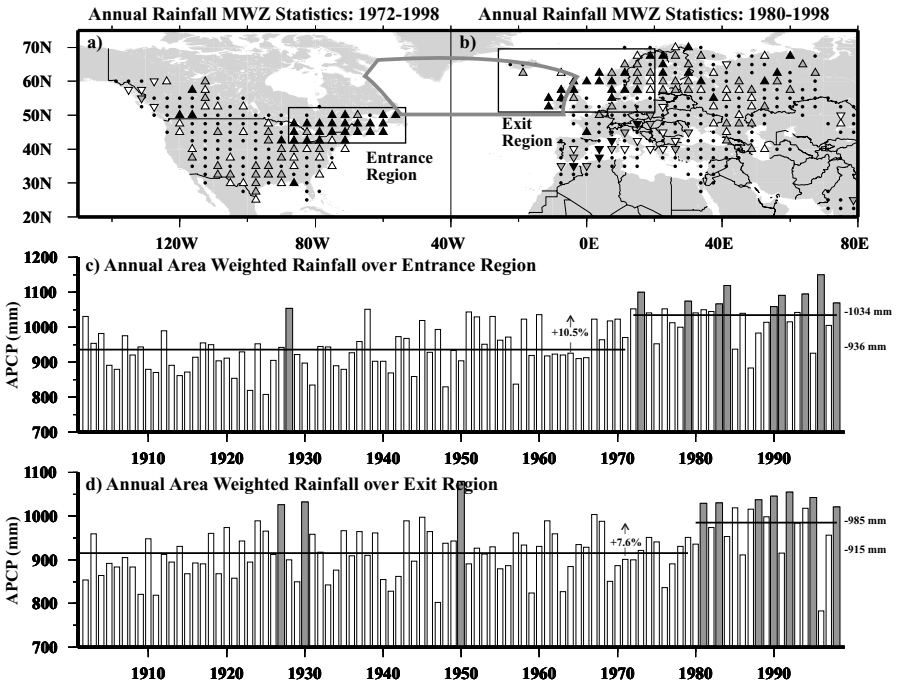

Fig. 13 (a) Mann Whitney Z statistics for annual rainfall rankings at North American grid locations during 1972–98. (b) Z statistics for annual rainfall rankings at European grid locations during 1980–98. The gray outlined North Atlantic area marks the sub-polar ocean basin of Curry and Mauritzen (2005). (c) October-September rainfall spatially averaged over the North Atlantic storm track entrance region outlined in (a) for 1901–98. Gray years mark the ten most highly ranked APCP values of 1901–98. Horizontal lines mark the mean annual precipitation for 1901–71 (936 mm) and 1972–98 (1034 mm). d) As in (c) for the North Atlantic storm track exit region outlined in (b) for 1901–98. Horizontal lines mark the mean annual precipitation for 1901–79 (915 mm) and 1980–98 (985 mm)

shift from NAO− to NAO+ conditions between the 1960's and 1990's, they propose that precipitation has increased over that area of the North Atlantic in recent decades. Using an 18 year data set of monthly rawinsonde data, they also demonstrate that NAO+ conditions are marked by an almost doubled poleward atmospheric moisture flux through that region during winter, relative to the 18 year winter mean. As a result, they suggest that the latent heat flux entering the European Arctic through the Nordic Seas has substantially increased since the 1960's.

When compared with some other long-term climatological data sets (e.g. Easterling et al. 1996) the precipitation data used here is relatively raw. That is, the data is not uniformly corrected for changes in gauge design or observing practices, or solid precipitation undercatch. While the recent North Atlantic precipitation mode suggested here is directly evident over North America and northern Europe, Hulme (1999) advises that variation in high latitude precipitation trends outside of Russia and Scandinavia be viewed with caution. As a result, the recent North American wetness detected with this data may be partly artificial, i.e., due in part to influences other than an actual increase in precipitation. But other evidence suggests a real climate effect. Groisman and Easterling's (1994) analysis of unbiased estimates of annual precipitation averaged over an area roughly coincident with

Figure 13a's entrance region shows a linear increase of +11.3% during 1891–1990, approximately equal to the +10.5% step-increase found in Figure 13c. As their data is adjusted for the effects of gauge undercatch, this suggests that that step increase is not the result of a late-century warm climate bias as described in Section 2. While the North American data used here is also uncorrected for instrumental discontinuities, consistent increases in annual mean streamflow over the Mississippi River valley and the eastern United States after the early 1970's (Mauget 2003, 2004) supports the position that Figure 13a's recent entrance region wetness, and North American wetness in general, is a true climate effect. Although the Hulme data may be relatively reliable over Scandinavia, the recent wetness over Figure 13b's exit region is also indirectly corroborated by the advance and increasing mass balance of glaciers in western Norway during the 1980's and 1990's (Tvede and Laumann 1997; Hoelzle et al. 2003), in contrast to the late-century retreat of glaciers evident in most other areas of the globe (Folland et al. 2001; Oerlemans 2005).

Results presented here and elsewhere suggest a strengthened hydrological cycle over the North Atlantic, possibly associated with the persistent positive state of the North Atlantic Oscillation in recent decades. Parts of this change are directly evident in data records of multi-decadal or longer time scales (e.g., this study; Mauget 2003; Curry et al. 2003; Hoeltzle et al. 2003), while other change is inferred from the recent tendency to NAO+ conditions and those conditions effects over ocean areas (Dickson et al. 2000). The overall pattern of change suggested here (Figure 14) is generally consistent with the clockwise, anti-cyclonic circulation of water vapor over major ocean basins (Manabe 1969). Although more recent modeling attempts to link late-century NAO+ conditions to increasing CO_2 concentrations have been inconclusive (Cubasch et al. 2001), Figure 14's pattern of change is also consistent with Manabe and Wetherald's (1980) early study of the effects of higher CO_2 levels on a simplified atmosphere-ocean general circulation model. That model consisted of a single northern Hemisphere ocean basin bordering a continent to the west, roughly analogous to the combined North Atlantic and North America region. Model integrations with doubled CO_2 levels resulted in increased transport of water vapor around the oceanic anticyclone. That increased moisture flux produced wetter conditions along the east coast of the model continent, increases in precipitation and runoff at higher latitudes, and a large increase in the poleward transport of water vapor and the associated latent heat energy.

The lack of long-term meteorological and oceanographic data over ocean regions makes it hard to identify low-frequency change in the hydrological cycle over those areas. This lack of context over time also makes determining the significance of such change uncertain. However, the recent North American and northern European terrestrial wet periods found here represent highly significant changes in precipitation in centennial time-scale records, relative to Section 3.1's definition of stationary climate variability (H_0). In terms of continuous and observable rainfall variation those multi-decadal wet periods were unprecedented over those areas during 1901–98. Given the 'brute force' nature of this study's climate survey approach and the sensitivity of the underlying time series analysis method, Table 1 shows that those wet regimes were unprecedented over all the land regions considered here during that time. It is suggested here that this recent and marked wetness bordering the North Atlantic may be the most observable evidence of a broader pattern of North Atlantic climate change. However, whether other elements of that change over ocean areas – increased evaporation and salinity over the subtropical North Atlantic, increased rainfall and decreased salinity at midlatitudes, and increased latent heat flux into polar regions – are comparably significant is open to question. But those elements could be important factors in climate change beyond the North Atlantic. That ocean region is a critical deep water formation area of the thermohaline

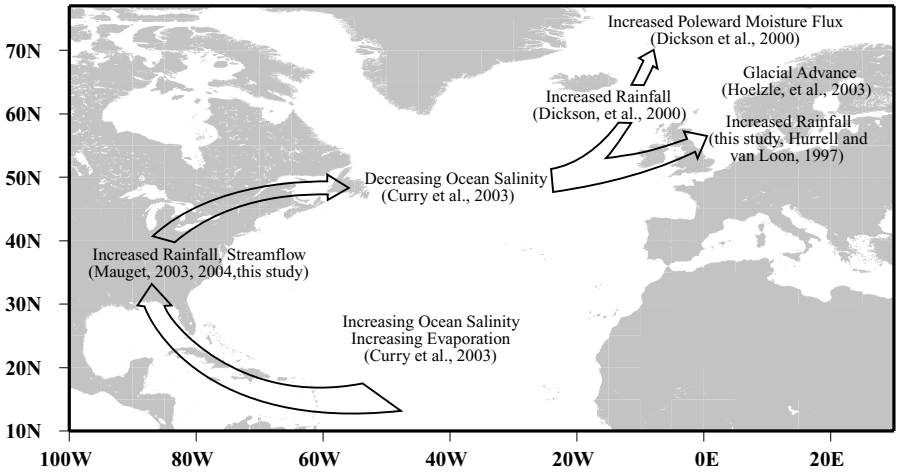

Fig. 14 The pattern of North Atlantic hydrological change suggested by the late 20th century North American and northern European rainfall regimes found here, and late century atmospheric and oceanographic change proposed by other studies. Arrows indicate the clockwise, anticyclonic sense of water vapor transport over major ocean basins

circulation, which may influence global climate (Dickson 1997; Broecker 1997). Also, the majority of latent heat flux into the Arctic occurs through North Atlantic sub-polar areas (Serreze et al. 1995; Dickson et al. 2000). Because of the relative magnitudes of the latent heats of condensation and fusion, one gram of water vapor condensing on an ice surface releases enough latent heat energy to, potentially, melt seven grams of ice. A significant increase in the poleward flux of this 'fluid sunshine' (Pierrehumbert 2002) could have an important effect on Arctic ice cover, with associated changes in the ice-albedo effect (Comiso and Parkinson 2004) and Arctic warming. While attribution studies indicate the primary role of greenhouse gas radiative forcing in the late 20th century trend of general surface warming (Lean et al. 1995; Lean and Rind 1998; Tett et al. 1999; Stott et al. 2000), a potential consequence of that warming is a stronger hydrological cycle (Trenberth 1999; Meehl et al. 2000; Cubasch et al. 2001). As a result, if Figure 14's oceanic components of change are similarly significant to the recent North American and northern European wet periods found here, then that overall North Atlantic climate shift may represent a leading-response of the Earth's hydrological system to that forcing.

Acknowledgements Thanks to preliminary reviewers Charles Jones and James Mahan. The precipitation data used here (Gu23wls0098.dat, Version 1.0) was constructed and supplied by Dr. Mike Hulme at the Climatic Research Unit, University of East Anglia, Norwich, UK. That work was supported by the UK Department of the Environment, Transport and the Regions (Contract EPG 1/1/85). All figures were produced using Generic Mapping Tools (Wessel and Smith, 1995).

References

Akaike H (1974) A new look at the statistical model identification. IEEE Trans Autom Control AC-19:716–723

Bradley RS, Diaz HF, Eischeid PD, Jones PD, Kelly PM, Goodess CM (1987) Precipitation fluctuations over northern hemisphere land areas since the mid-19th Century. Science 237:171–175

Broecker WS (1997) Thermohaline circulation, the Achilles Heel of our climate system: Will man-made CO_2 upset the current balance? Nature 278:1582–1588
Broecker WS, Denton GH (1989) The role of ocean-atmosphere reorganizations in glacial cycles. Geochim Cosmochim Acta 53:2465–2501
Comiso JC, Parkinson CL (2004) Satellite-observed changes in the Arctic. Physics Today 57:38–44
Cubasch U, Meehl GA, Boer GJ, Stouffer RJ, Dix M, Noda A, Senior CA, Yap KS, Contributing Authors (2001) Projections of Future Climate Change. In: Houghton JT, Ding Y, Griggs DJ, Noguer M, van der Linden PJ, Dai X, Maskell K, Johnson CA (eds), Climate Change 2001: The Scientific Basis Contribution of Working Group I to the Third Assessment Report of the Intergovernmental Panel on Climate Change. Cambridge Univercity Press, Cambridge, pp 525–582
Cullen HM, deMenocal PB (2000) North Atlantic influence on Tigris-Euphrates streamflow. Int J Climatology 20:853–863
Cullen HM, Kaplan A, Arkin PA, deMenocal PB (2002) Impact of the North Atlantic Oscillation on Middle Eastern climate and streamflow. Climatic Change 55:315–338
Curry R, Dickson B, Yashayaev I (2003) A change in the freshwater balance of the Atlantic Ocean over the past four decades. Nature 426:826–829
Curry R, Mauritzen C (2005) Dilution of the northern North Atlantic Ocean in recent decades. Science 308:1772–1774
Dai A, Fung IY, Del Genio AD (1997) Surface observed global land precipitation variations during 1900–1988. J Climate 10:2943–2962
Diaz HF, Bradley RS, Eischeid JK (1989) Precipitation fluctuations over global land areas since the late 1800's. J Geo Res 94:1195–1210
Dickson RR, Meincke J, Malmberg SA, Lee AJ (1988) The "Great Salinity Anomaly" in the northern North Atlantic 1968–1982. Progress in Oceanography 38:241–295
Dickson RR (1995) The local, regional, global significance of exchanges through the Denmark Strait and Irminger Sea. In: Natural Climate Variability on Decade to-Century Time Scales. National Academy Press, Washington DC, pp 305–317
Dickson RR (1997) From the Labrador Sea to global change. Nature 386:649–650
Dickson R, Osborn TJ, Hurrell JW, Meincke J, Blindheim J, Adlandsvik B, Vinje T, Alekseev G, Maslowski W (2000) The Arctic Ocean response to the North Atlantic Oscillation. J Climate 13:2671–2696
Dickson B, Yashayaev I, Meinke J, Turrell B, Dye S, Holfort J (2002) Rapid freshening of the deep North Atlantic over the past four decades. Nature 416:832–837
Easterling DR, Horton B, Jones PD Peterson TC, Karl TR, Parker DE, Salinger MJ, Rasuvayev V, Plummer N, Jamason P, Folland CK (1994) Maximum and minimum temperature trends for the globe. Science 277:364–367
Easterling DR, Karl TR, Mason EH, Hughes PY, Bowman DP, Daniels RC, Boden TA (eds): (1996) United States Historical Climatology Network (US HCN) Monthly Temperature and Precipitation Data ORNL/CDIAC-87, NDP-019/R3 Carbon Dioxide Information Analysis Center. Oak Ridge National Laboratory, Oak Ridge, Tennessee
Eshel G, Cane MA, Farrell BF (2000) Forecasting eastern Mediterranean droughts. Mon Wea Rev 128:3618–3630
Folland CK, Karl TR, Christy JR, Clarke RA, Gruza GV, Jouzel J, Mann ME, Oerlemans J, Salinger MJ, Wang S-W, Contributing Authors (2001) Observed Climate Variability and Change. In: Houghton JT, Ding Y, Griggs DJ, Noguer M, van der Linden PJ, Dai X, Maskell K, Johnson CA (eds), Climate Change 2001: The Scientific Basis Contribution of Working Group I to the Third Assessment Report of the Intergovernmental Panel on Climate Change. Cambridge Univ. Press, Cambridge, pp 99–181
Groisman PY, Koknaeva VV, Belokrylova TA, Karl TR (1991) Overcoming biases of precipitation measurement: A history of the USSR experience. Bull Amer Meteor Soc 72:1725–1733
Groisman PY, Legates DR (1995) Documenting and detecting long-term precipitation trends: Where we are and what should be done. Climatic Change 31:601–622
Groisman PY, Easterling DR (1994) Precipitation changes over the northern hemisphere extratropics during the last hundred years. In: Desbois M, Desalmand F (eds), Global Precipitations and Climate Change. Springer-Verlag, Berlin, pp 119–133
Häkkinen S (2002) Freshening of the Labrador Sea surface waters in the 1990s: Another great salinity anomaly? Geo Res Lett 29:85-1–85-4 (doi:101029/2002GL015243, 2002)
Hansen DV, Bezdek HF (1996) On the nature of decadal anomalies in North Atlantic sea surface temperature. J Geo Res 101:8749–8758
Hansen J, Ruedy R, Sato M, Imhoff M, Lawrence W, Easterling D, Peterson T, Karl T (2001) A closer look at United States and global surface temperature change. J Geo Res 106:23947–23963
Hartmann DL (1994) Global physical climatology. Academic Press, San Diego, 411pp

Hoelzle M, Haeberli W, Dischl M, Peschke W (2003) Secular glacier mass balances derived form cumulative glacier length changes. Gl Plan Change 36:295–306
Hulme M (1992) A 1951–80 global land precipitation climatology for the evaluation of general circulation models. Climate Dyn 7:57–72
Hulme M (1994) Validation of large-scale precipitation fields in General Circulation Models Global Precipitation and Climate Change. In: Desbois M, Desalmand F (eds), NATO ASI Series. Springer-Verlag, Berlin, pp 387–406
Hulme M, Osborne TJ, Johns TC (1998) Precipitation sensitivity to global warming: Comparisons of observations with HadCM2 simulations. Geo Res Lett 25:3379–3382
Hulme M (1999) gu23wld0098dat, Version 10, at http://www.cru.uea.ac.uk/∼mikeh/datasets/global/gu23wld0098_docpdf
Hurrell JW (1995) Decadal trends in the North Atlantic Oscillation: Regional temperatures and precipitation. Science 269:676–679
Hurrell JW, van Loon H (1997) Decadal trends in climate associated with the North Atlantic Oscillation. Climatic Change 36:301–326
Hurrell JW, Kushnir Y, Ottersen G, Visbeck M (2003) An overview of the North Atlantic Oscillation. In: Hurrell JW, Kushnir Y, Ottersen G, Visbeck M (eds), The North Atlantic Oscillation: Climatic Significance and Environmental Impact, Geophysical Monograph 134. American Geophysical Union, Wash DC, pp 1–35
Jones PD, New M, Parker DE, Martin S, Rigor IG (1999) Surface air temperature and its changes over 150 years. Rev Geophys 37:173–199
Lau KM, Weng H (1995) Climate signal detection using wavelet transform: How to make a time series sing. Bull Amer Meteor Soc 76:2391–2402
Lean J, Beer J, Bradley R (1995) Reconstruction of solar irradiance since 1610: implications for climate change. Geophys Res Lett 22:3195–3198
Lean J, Rind D (1998) Climate forcing by changing solar radiation. J Climate 11:3069–3094
Levitus S, Antonov JI, Wang J, Delworth TL, Dixon W, Broccoli AJ (2001) Anthropogenic warming of the Earth's climate system. Science 292:267–270
Lins HF, Slack JR (1999) Streamflow trends in the United States. Geophys Res Let 26:227–230
Mann HB, Whitney DR (1947) On a test of whether one of two random variables is stochastically larger than the other. Ann Math Statist 18:50–60
Manabe S (1969) Climate and ocean circulation: I. The atmospheric and the hydrology of the earth's surface. Mon Wea Rev 97:739–774
Manabe S, Wetherald RT (1980) On the distribution of climate change resulting from an increase in CO_2 content of the atmosphere. J Atmos Sci 37:99–118
Mauget S (2003) Multidecadal regime shifts in US streamflow, precipitation and temperature at the end of the twentieth century. J Climate 16:3905–3916
Mauget S (2004) Low frequency streamflow regimes over the central United States: 1939–1998. Climatic Change 63:121–144
McCabe G J, Wolock DM (2002) A step increase in streamflow in the conterminous United States. Geophys Res Lett 29:2185–2188
Meehl GA, Zweirs F, Evans J, Knutson T, Mearns L, Whetton P (2000) Trends in extreme weather and climate events: Issues related to modeling extremes in projections of future climate change. Bull Amer Meteor Soc 81:427–436
Mendenhall W, Wackerly DD, Sheaffer RL (1990) Mathematical Statistics with Applications. PWS-Kent, Boston, p 688
National Research Council (2002) Abrupt Climate Change: Inevitable Surprises. National Academy Press, Washington, DC, pp 61–65
Nicholls N, Gruza GV, Jouzel J, Karl TR, Gruza GV, Jouzel J, Ogallo LA, Parker DE, Contributing Authors (2001) Observed Climate Variability and Change. In: Houghton JT, Meiro Filho LG, Callendar BA, Kattenberg A, Maskell K (eds), Climate Change 1995: The Science of Climate Change. Cambridge Univ. Press, Cambridge, pp 133–192
Oerlemans J (2005) Extracting a climate signal from 169 glacier records. Science 308:675–677
Parker DE, Jones PD, Folland CK, Bevan A (1994) Interdecadal changes of surface temperature since the late 19th century. J Geo Res 99:14373–14399
Peterson TC, Easterling DR, Karl TR, Groisman P, Co-Authors: (1998) Homogeneity adjustments of *in situ* atmospheric climate data: a review. Int J of Climatology 18:1493–1517
Pierrehumbert RT (2002) The hydrological cycle in deep-time climate problems. Nature 372:191–198
Rahmstorf S (1997) Rapid climate transitions in a coupled ocean-atmosphere model. Nature 372:82–85
Ramaswamy V, Boucher O, Haigh J, Hauglastaine D, Haywood J, Myhre G, Nakajima T, Shi GY, Solomon S, Contributing Authors (2001) Radiative Forcing of Climate Change. In: Houghton JT, Ding Y, Griggs DJ,

Noguer M, van der Linden PJ, Dai X, Maskell K, Johnson CA (eds), Climate Change 2001: The Scientific Basis Contribution of Working Group I to the Third Assessment Report of the Intergovernmental Panel on Climate Change. Cambridge Univ. Press, Cambridge, pp 349–416

Rind D, Shindell D, Perlwitz J, Lerner J, Lonergan P, Lean J, McLinden C (2004) The relative importance of solar and anthropogenic forcing of climate change between the Maunder Minimum and the present. J Climate 17:906–928

Rogers JC (1990) Patterns of low frequency monthly sea pressure variability (1899–1986) and associated wave cyclone frequencies. J Climate 3:1364–1379

Rogers JC (1997) North Atlantic storm track variability and its association to the North Atlantic Oscillation and climate variability of northern. Europe J Climate 10:1635–1647

Rothrock DA, Yu Y, Maykut GA (1999) Thinning of the Arctic sea-ice cover. Geophys Res Let 26:3469–3472

Schlesinger ME, Ramankutty N (1994) An oscillation in the global climate system of period 65–70 years. Nature 367:723–726

Sellers WD (1965) Physical climatology. University of Chicago Press, Chicago

Serreze MC, Barry RG, Walsh JE (1995) Atmospheric water vapor characteristics at 70° N. J Climate 8:719–731

Serreze MC, Walsh JE, Chapin III FS, Osterkamp T, Dyurgerov M, Romanovsky V, Oechel WC, Morison J, Zhang T, Barry RG (2000) Observational evidence of recent change in the northern high-latitude environment. Climatic Change 46:159–207

Stocker TF, Wright DG (1991) Rapid transitions of the ocean's deep circulation induced by changes in surface water fluxes. Nature 351:729–732

Stott PA, Tett SFB, Jones GS, Allen MR, Mitchell JFB, Jenkins GJ (2000) External control of 20th century temperature by natural and anthropogenic forcings. Science 290:2133–2137

Sutton RT, Allen MR (1997) Decadal predictability of North Atlantic sea surface temperature and climate. Nature 388:563–567

Tett SFB, Stott PA, Allen MR, Ingram WJ, Mitchell JFB (1999) Causes of twentieth-century temperature change near the Earth's surface. Nature 399:569–572

Thiebaux HJ, Zwiers FW (1984) The interpretation and estimation of effective sample size. J Clim Appl Meteorol 23:800–811

Trenberth KE (1999) Conceptual framework for changes of extremes of the hydrological cycle with climate change. Clim Change 42:327–339

Trenberth KE, Dai A, Rasmussen RM, Parsons DB (2003) The changing character of precipitation. Bull Amer Meteor Soc 84:1205–1217

Tvede AM, Laumann T (1997) Glacial variations on a meso-scale: examples from glaciers in the Aurland Mountains, southern Norway. Ann Glaciol 24:130–134

Vinnikov KY, Groisman PY, Lugina KM (1990) Empirical data on contemporary global climate changes (temperature and precipitation). J Climate 3:662–677

Visbeck M, Chassignet EP, Curry RG, Delworth TL, Dickson RR, Krahmann G (2003) The Oceans's Response to North Atlantic Oscillation Variability. In: Hurrell JW, Kushnir Y, Ottersen G, Visbeck M (eds), The North Atlantic Oscillation: Climatic Significance and Environmental Impact, Geophysical Monograph 134. American Geophysical Union, Wash DC, pp 113–145

Wessel P, Smith WHF (1995) New Version of the Generic Mapping Tools Released' EOS. Trans Am Geophys Union 76:329

Wilcoxon F (1945) Individual comparisons by ranking methods. Biometrics Bull 1:80–83

Wilks DS (1995) Statistical Methods in the Atmospheric Sciences. Academic Press: San Diego, p 139

Xie P, Arkin PA (1996) Global precipitation: A 17-year monthly analysis based on gauge observations, satellite estimates, numerical model outputs. Bull Amer Meteor Soc 78:2539–2558